



H2020 MARIE SKŁODOWSKA-CURIE ACTIONS



**Smart Mitigation of flow-induced Acoustic Radiation
and Transmission for reduced Aircraft, surface traNSport,
Workplaces and wind enERgy noise**

Grant Agreement No 722401

D3.2 – Interim WP3 report

Low-transmission: interim public report

Authors: Felipe Alves Pires, Emanuele De Bono, Thomas Laurence

Due date: December 31st, 2018

This document is property of the SmartAnswer Consortium
and shall not be distributed without prior consent of its Beneficiaries.

Table of Contents

1. Introduction.....	2
2. Investigation of sound transmission loss of vibro-acoustic metamaterials.....	2
2.1. Positioning with respect to previous work on vibro-acoustic metamaterials.....	2
2.1.1. Unit cell and Resonance based stop bands	3
2.1.2. Exploiting the resonator’s footprint.....	5
2.1.3. Moving from infinite structures to finite structures.....	7
2.2. Realizable vibro-acoustic metamaterials with different footprints	8
2.2.1. Host structure	9
2.2.2. Designed resonators	10
2.2.3. Realizable resonators	12
2.2.4. Experimentally testing the beams	14
2.3. Concluding remarks	17
3. References.....	17

1. Introduction

The development of low-transmission technologies applied to reducing noise and vibrations in sectors such as automotive and aerospace have gained major attention in the last decades. This deliverable focuses on metamaterials for improved sound transmission loss of panels to bring low transmission technology closer to transport applications. Originally this deliverable was supposed to also report on the potential of architected non-linear materials for achieving broadband efficient attenuation. However, since the potential of linear materials was still not fully investigated, focused was kept on these linear materials, as reported both in this deliverable as well as in deliverable 2.2.

2. Investigation of sound transmission loss of vibro-acoustic metamaterials

This section aims at showing the potential of vibro-acoustic metamaterials as a solution to vibro-acoustic transmission problems. Particularly, the investigation will focus on assessing the metamaterials footprint and its influence on the metamaterial performance in a vibrational point of view.

2.1. Positioning with respect to previous work on vibro-acoustic metamaterials

The development of novel Noise, Vibration and Harshness (NVH) solutions for engineering applications is of key importance and due to trends towards the use of lightweight structures, novel low mass and low volume NVH solutions are necessary in order to tackle the challenges of not only achieving a good NVH reduction performance but also attending the lightweight

requirements. Metamaterials have been investigated and proven to hold great potential to enhance the vibro-acoustic response of several engineering applications [1] [2] [3] [4], since they can create stop bands, or band gaps, which are frequency zones where there is no propagation of waves. For more information about metamaterials, the reader is kindly referred to the D3.1 Low-transmission: state-of-the-art and potential synthesis report.

Various parameters and conditions have been shown to have an effect on these stop bands such as damping properties of the constituent materials and the shape of these metamaterial inclusions [5] [6]. Additionally, the influence of boundary conditions and the way they affect stop bands have also been investigated [7]. This report has the aim to investigate another parameter that could have an influence on resonance based stop bands: the contact area between the resonant addition and the host structure, in other words, the footprint that the resonators have on the structure. This feature will be studied by investigating 1D metamaterial beams. At first, some theoretical insights will be given by using TVAs (tuned vibration absorbers) and later experimental results will be shown in order to verify if the considered theoretical approach illustrates the reality when a real life application is examined.

2.1.1. Unit cell and Resonance based stop bands

Stop bands can be achieved by tuning resonant additions to a targeted frequency which will form a stop band in the frequency region around the resonance frequency of the resonant addition. In order to improve NVH behavior, the stop bands are designed to block the propagation of flexural waves.

In order to help understand this concept, the most basic example of a resonant system can be taken: a TVA (tuned vibration absorber), as shown in Figure 1. These systems can be understood as single degree of freedom mass-spring systems (SDOF) and frequently, due to the existence of a localized resonance in the UC, it can lead to a stop band whose designs are often based on UC models, which represent infinite structures [8][9].

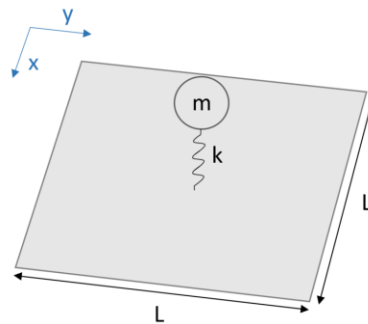


Figure 1: SDOF mass-spring system on a UC of length L.

Dispersion diagrams are often used to predict the stop band frequencies. The methodology involves a UC modeling as well as the application of Bloch's theorem and Brillouin zones, as stated before. A hypothetical test case will be used to illustrate how to verify and interpret a dispersion diagram. The test case will consider a host structure made of steel with a unit cell of length $L = 50$ mm and thickness $t = 5$ mm. The material properties are shown in Table 1. The resonant addition will be tuned to 2000 Hz in order to be in a sub-wavelength scale, with a

frequency ratio $f_{\text{res}}/f_{\lambda/2} = 0.4$ [1][10], considering 20% of mass addition by the TVA w.r.t the UC mass. Equation 1 accounts for $f_{\lambda/2}$, which is the frequency where the structural wavelength equals twice the UC length for infinite plates

$$f_{\frac{\lambda}{2}} = \frac{\pi}{2L^2} \sqrt{\frac{t^2 E}{12(1-\nu^2)\rho}} \quad (1)$$

where E , ρ and ν are Young's modulus, density and Poisson's ratio of the used material, respectively.

Table 1: Material properties of steel.

Young's Modulus	Density	Poisson's Ratio
210 GPa	7800 kg/m ³	0.3

Figure 2 illustrates the dispersion diagram of the test case. Dispersion diagrams describe the wave propagation in terms of wavenumber and frequency. The y-axis represents the frequencies in which the waves are propagating and the x-axis the wavenumber. The curves indicate for which frequencies free wave propagation can be found in certain direction and with certain wave numbers. The dashed black and solid orange lines account for the dispersion curves for the case without any TVAs and with TVAs, respectively. It can be seen that no free wave propagation is found for the frequency to which the TVA was tuned to, indicating a resonance based stop band. It ranges from 1956 – 2172 Hz, being 216 Hz wide. The points O-A-B-O represent the Irreducible Brillouin Contour (IBC) [11] and they consist of propagation vectors in the dimensionless wave domain, that is $(0,0) - (0,\pi) - (\pi,\pi) - (0,0)$, respectively, which is obtained by scaling the wave vectors with the unit cell length.

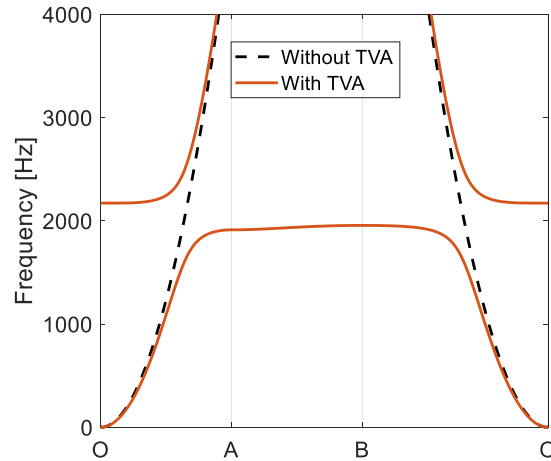


Figure 2: Dispersion diagram of the test case.

2.1.2. Exploiting the resonator's footprint

So far, the working principle of resonance based stop bands has been shown. This section has the aim to investigate how the footprint of the resonator inside the UC, in other words, the area that the resonator occupies inside the UC, affects the stop bands.

At first, TVAs will be again used in order to gain insight about a resonator's footprint. Particularly, modified TVAs will be utilized. These modified TVAs are basically SDOF systems but with extra added springs, instead of having only one spring as shown in Figure 1. As an example, Figure 3 illustrates a modified TVA which occupies a square area. When more springs are added, the resonator no longer occupies one point, but it covers a bigger area inside the UC. It is worth mentioning that, in this analysis, the amount of added mass by the resonant addition will be kept the same and the total stiffness of all springs will be kept the same such that always the same tuned resonance frequency is achieved, since the springs are considered to be in parallel to each other. The stiffness k of each spring will be $k_{\text{new}} = k_{\text{original}}/n$, where n is the number of added springs and k_{original} is the stiffness of the original spring.

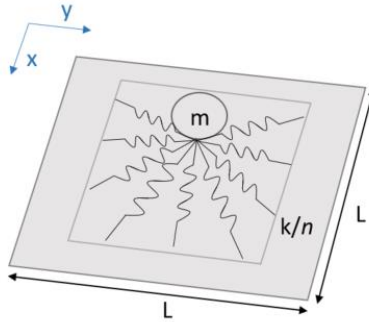


Figure 3: Modified SDOF mass-spring system on a UC of length L occupying a square area.

As a way of quantifying this footprint, values of percentage will be used according to the area the addition occupies in the UC. For instance, a 1-spring TVA as in Figure 1 will be evaluated as having 0% of footprint, as they are fixed only in one point. Similarly, a modified resonator that occupies a square area of 80% w.r.t. the entire area of the UC, will be evaluated as having 80% of footprint, e.g. if $A_{\text{UC}} = 50 \times 50 \text{ mm}^2$, the area that the resonator occupies is $A_{\text{res}} = 40 \times 40 \text{ mm}^2$. Hence, as the value of footprint increases, the number of springs also increases.

As an example, Figure 4 illustrates the stop bands created by using a modified TVA with 80% of footprint compared to the first case, tuned to the same frequency of 2000 Hz and with same mass addition. It can be seen that, even though the TVA is tuned to the same frequency as before, the stop band region is slightly shifted to higher frequencies. In this case ranging from 1991 - 2191 Hz, being 200 Hz wide and, consequently, 16 Hz narrower compared to the first case. This happens due to the distribution of forces by the TVA throughout the UC.

In the case with 1 spring, the contributing force is concentrated in 1 point, which is not the case when more springs are added since the resonator's contributing forces are distributed in a larger

area. Furthermore, this approach provides an analysis closer to real-life applications since in reality there would not be a resonant addition occupying only one point on the host structure but resonators that occupy a certain area in the system.

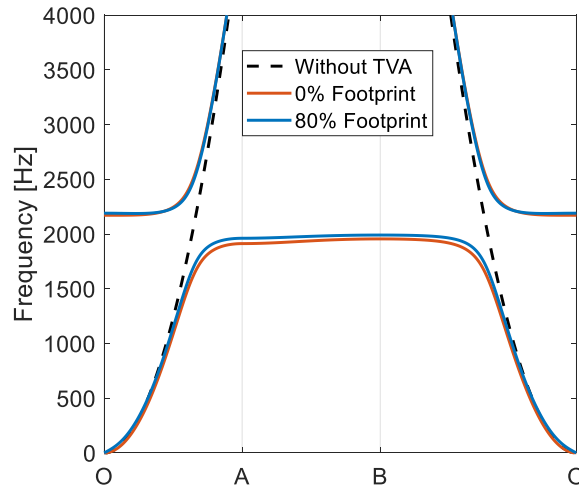


Figure 4: Comparison between dispersion diagrams between 0% and 80% of footprint resonators.

This example helped gaining insights about the idea behind studying the footprint of resonators inside the UC. Thus, another analysis was performed by changing the UC length L , which was fixed in 50 mm in the test case. Same conditions were applied, by tuning the resonators to 2000 Hz and keeping 20% of mass addition. Figure 5 shows the comparison of stop bands versus footprint ratio for different UC lengths.

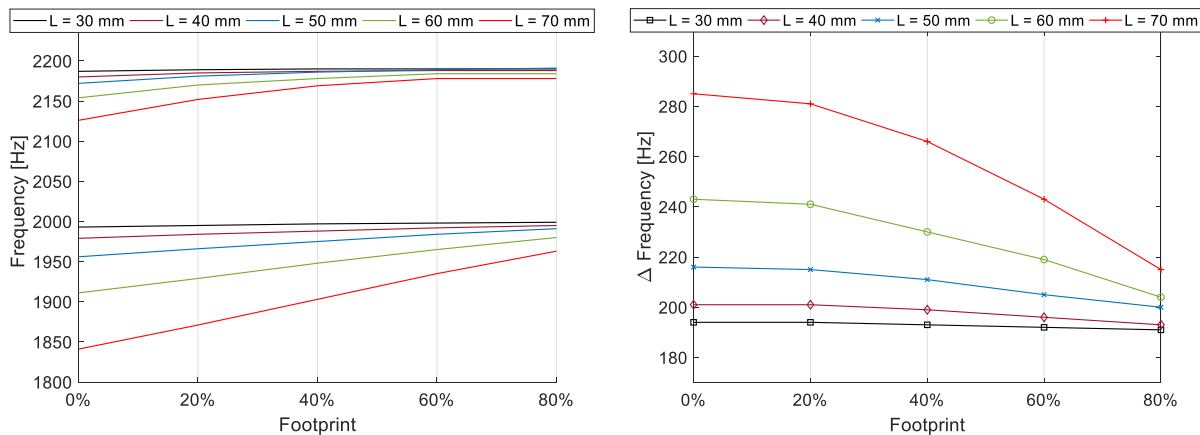


Figure 5: Comparison of stop bands as a function of the footprint for different UC lengths (Left) Stop band limits (Right) Stop band widths.

By analyzing these 2 graphs together, it can be seen that there is a trend towards wider stop bands as L increases and this is due to the fact that the value of $f_{N/2}$ reduces as the unit cell length grows, which results in a combination of interference based and resonance based stop bands[10]. Another

common trend is the fact that the stop bands' widths decrease as the footprints increase, as introduced earlier in this report. This trend can be seen clearly for the case $L = 70$ mm, whose high frequency ratio is high. Therefore, it can be concluded that the footprint that the resonant additions have inside the UC have some influences on the stop bands and this feature needs to be taken into account when designing realizable resonators. Thus, in order to have the wider stop bands, the resonant additions' footprint need to be as small as possible.

2.1.3. Moving from infinite structures to finite structures

Nonetheless, just infinite structures have been analyzed. It is also of significant importance to investigate the effect of stop bands as well as the footprint on finite problems. This section has the aim to gain insight about the link between the stop bands predicted by dispersion diagrams of infinite structures and equivalent finite structures [10], also exploiting resonators of different footprints by using numerical examples.

In this section, a finite plate made of steel is derived from the repetition of 6×8 unit cells of $L = 50$ mm, as addressed earlier, therefore, having as dimensions $300 \times 400 \times 5$ mm. The applied boundary condition will be simply supported along its boundaries. A harmonic point force of 1 N of magnitude will be applied at a point with coordinates (0.115,0.105). The 2 types of TVAs with different footprints already explored in this report will be used to check also not only the influence on the stop bands but also on the finite plate response due to the excitation. In addition, this analysis considers 1% of structural damping for the plate's material and 1% of viscous damping for the TVAs.

The responses due to the point force excitation will be evaluated in terms of velocity (m/s) in 120 randomly chosen points on the plate. Figure 6 shows an example of a plate with resonators of 80% of footprint tuned to 2000 Hz, adding 20% of mass w.r.t the mass of the plate. The blue arrow pointing downwards represents the point of excitation.

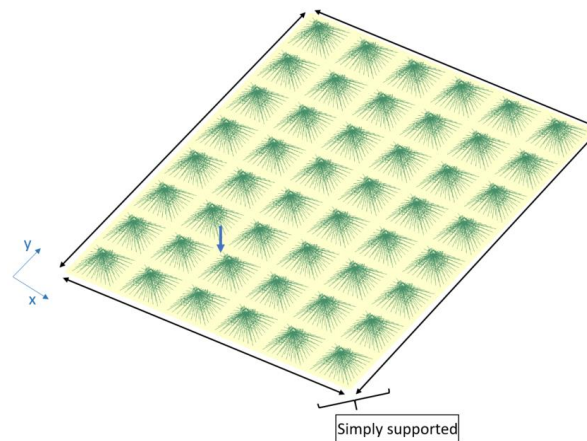


Figure 6: Structural set-up for a plate with modified TVAs.

In total, 3 simulations were performed: one to retrieve the response of the bare panel, one for the plate with added 0% footprint resonators and, lastly, one to verify the structural response with added 80% footprint resonators. Figure 7 illustrates the frequency response functions (FRFs) for the present plate. The black, orange and blue solid lines represent the FRFs for the bare case, plate

with 0% footprint resonators and plate with 80% footprint resonators, respectively, in terms of root mean square (RMS) velocity. Green and red solid vertical lines account for the previously predicted stop bands for the respective resonant additions.

From the figure, improvements in the structure's response can be seen around the frequency range where the stop bands were predicted. Pronounced dips can be noticed in both vibratory responses of the plate. One trend can be the fact that these dips tend to shift to higher frequencies as the footprint increases. Clearly, before the predicted stop bands, the response related to the TVAs with 0% of footprint has lower levels compared to the second case. Furthermore, the frequency region with pronounced attenuation is bigger for the first case when also compared to the latter.

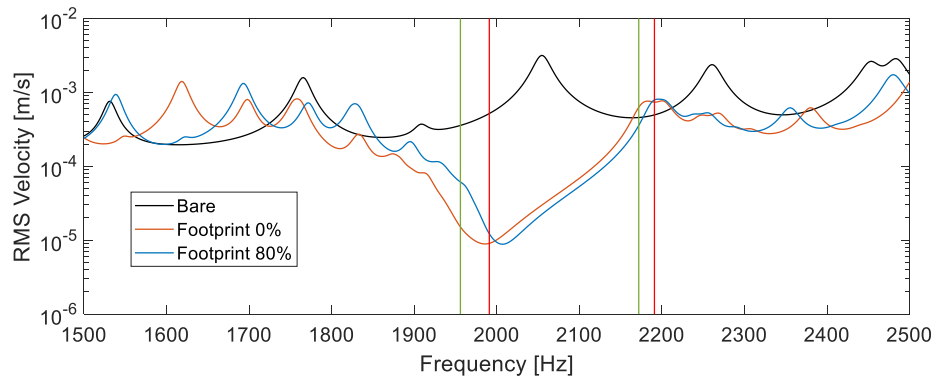


Figure 7: FRF of a finite plate with resonant additions of different footprints.

This section helped to understand the influence of the resonant additions' footprint on stop bands and the responses of finite problems as well as the reason why this footprint needs to be taken into account when designing and applying metamaterials. However, the analyses performed so far utilized only theoretical structures e.g. SDOF resonant structures. With this in mind, there is the need of verifying whether the caught trends can also be found in a real-life metamaterial application. This investigation will be the topic of the next section.

2.2. Realizable vibro-acoustic metamaterials with different footprints

As seen in the previous section, the resonant addition's footprint seems to influence the predicted stop bands, not only their location but also their widths as well as the frequency response of a finite structure due to an excitation. This section has the goal of verifying experimentally the influence of the footprint on the predicted stop bands and on the response of a finite structure with attached real-life metamaterial additions.

In order to carry out this study, resonators will be designed in a certain way so it is possible to easily change their footprints. Basically, the parameter that will change is the length of their base so that their footprints can be either increased or decreased. These resonators will be attached to finite beams. This design approach was chosen because of its ease of analysis and manufacturability.

The derived resonators will be designed with same features e.g. resonance frequency, added mass and effective mass and applied to beams made of aluminum. The RMS velocities from several sections will be acquired by using a PSV 500 laser vibrometer.

2.2.1. Host structure

In order for validating the footprint story, experiments will be performed in beams made of aluminum. In total, 4 beams will be used: 1 as a bare case and 3 others with resonators of different footprints. These beams have dimensions 1064 x 30 x 2 mm and they were cut from the same source panel so the material properties are retained in all cases. Unit cells of dimensions 40 x 30 x 2 mm will be used in this particular case. Figure 8 illustrates the beam properties used in the model and in the experiments. The boundary conditions applied to the beams are clamped-free, so one end will be clamped and the other free. When clamped, these beams have a free length of 800 mm.

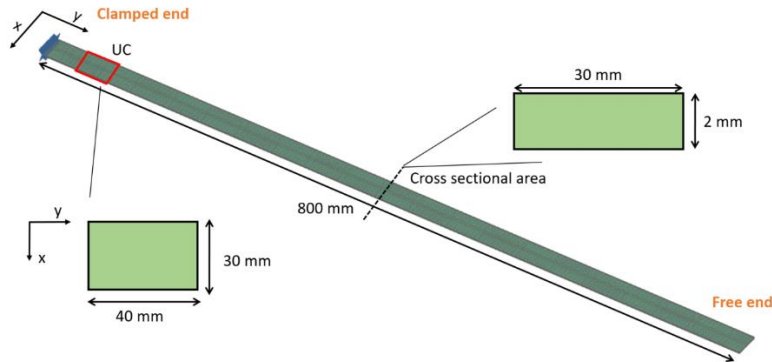


Figure 8: Beam properties used in the model and in the experiments.

A modal analysis was performed in a clamped bare beam so it was possible to retrieve the material properties of the aluminum, shown in Table 2.

Table 2: Material properties of the beam.

Young's Modulus	Density	Poisson's Ratio	% Structural Damping
63.14 GPa	2640.80 kg/m ³	0.34	0.01%

The beams will be divided into sections. These sections will be used to acquire the responses due to the excitation. In total, the responses will be evaluated in 20 sections throughout the beam. Three pieces of reflective tape were glued in each section with the aim of acquiring the responses in these 3 points (2 in the edges and 1 in the center), as illustrated in Figure 9.

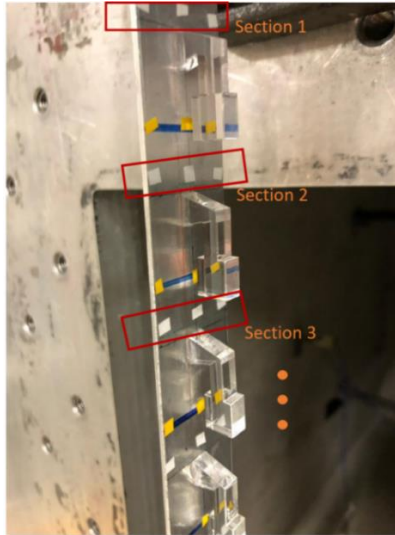


Figure 9: Sections in a metamaterial beam.

2.2.2. Designed resonators

The proposed resonators will be designed with the premise that as the footprint increases, the distribution of forces by the resonators on the unit cell also increases. With this in mind, they will be designed to be in sub-wavelength in a frequency ratio of 0.6, in this case. This frequency ratio has also been explored in another text [12]. The half-wavelength frequency for this case is $f_{\lambda/2} = 2865.4$ Hz, therefore, the targeted frequency is 1670 Hz.

Figure 10 illustrates the derived designs of the resonators. They will be addressed as resonators type 1, 2 and 3. Resonators type 1 have a smaller base so they have the smallest footprint compared to resonators types 2 and 3, with the latter having the biggest base amongst them, therefore, the biggest footprint. All of them are made of plexiglass and are 6 mm thick. The material properties of the resonators can be seen in Table 3, in which have been derived in other studies [1] [3]. Since the analysis will be carried out in beams, just the footprint in one direction will be considered, which differs from the approach used in the first section where a plate was chosen as a test case, however, same trends are expected.

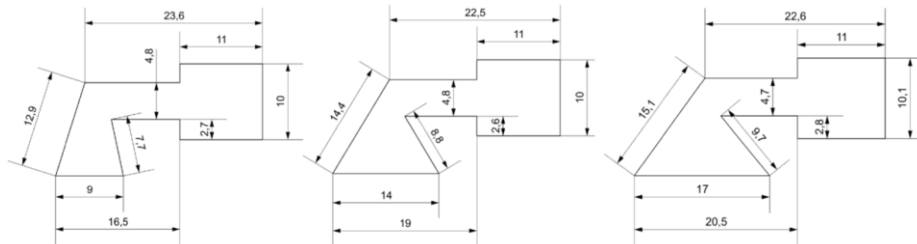


Figure 10: Resonators (Left) Type 1 (Center) Type 2 (Right) Type 3.

Table 3: Material properties of the resonators.

Young's Modulus	Density	Poisson's Ratio	% Structural Damping
4850 MPa	1188.38 kg/m ³	0.31	5%

As mentioned before, these resonators were designed so that it would be possible to get a bigger distribution of forces by these resonators on the UC as the footprint increases. This distribution of forces is depicted in Figure 11. This analysis results from verifying the first flexural eigenmode with the resonators fully clamped on their base. It shows that as the length of the base/footprint increases, these forces are more distributed on the unit cell.

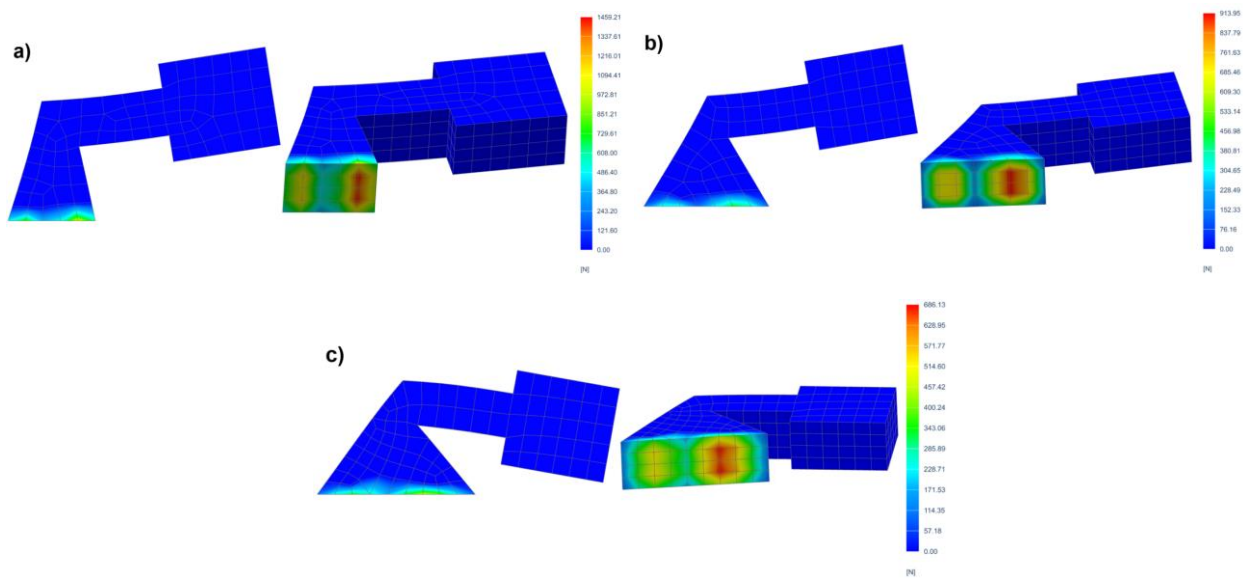


Figure 11: Distribution of forces by the resonators a) Type 1 b) Type 2 c) Type 3.

In this report, the stop bands of the infinite structures are predicted by using a UC modeling in combination with Bloch-Floquet boundary conditions and an undamped finite element approach, so the UC can be modeled to assess the wave propagation in the 1D waveguide systems [13] [14][15][16] . Figure 12 illustrates the predicted stop bands for the respective designs.

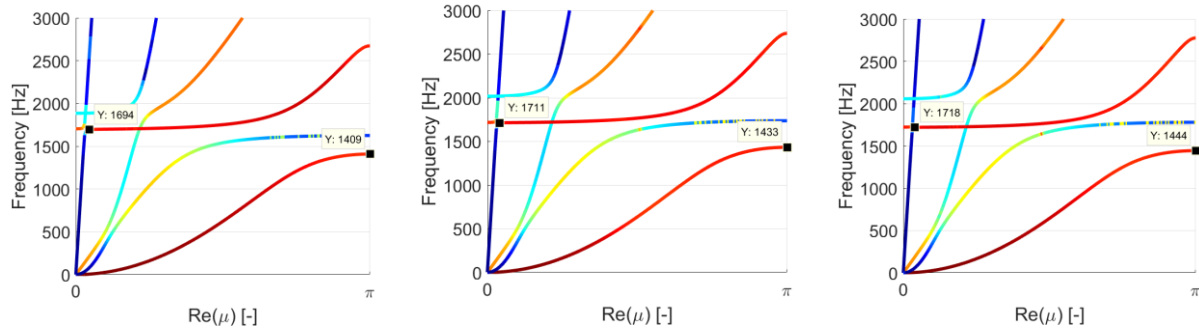


Figure 12: Predicted stop bands for the resonators (Left) Type 1 (Center) Type 2 (Right) Type 3.

Table 4 illustrates the details of each resonator. It shows that the resonators were designed to have close characteristics such as tuned frequency, percentage added mass and modal effective mass as the footprint changes. As expected, resonator type 3 has the narrowest stop band width compared to the others since the footprint in this case is the biggest. On the other hand, resonator type 1 owns the widest stop band width since this resonator has the smallest footprint.

Table 4: Resonators features numerically acquired.

Features	Resonator 1	Resonator 2	Resonator 3
Resonance Frequency [Hz]	1673.97	1669.97	1672.93
Static mass [g]	1.6241	1.7289	1.8362
Added mass	25%	26.75%	28%
Effective mass [g]	0.8504	0.8491	0.8584
SB limits [Hz]	1409 - 1694	1433 - 1711	1444 - 1718
SB Widths [Hz]	285	278	274
Footprint	22.50%	35%	42.50%

2.2.3. Realizable resonators

The aforementioned resonators were laser cut. Examples of the laser cut resonators are shown in Figure 13. In order to check if the resonance frequency of the laser cut resonators match to the ones numerically predicted, 12 resonators of each type were tested by gluing them to a metal block, rigidly connected to the stinger of a shaker. The velocity at the tip of the resonator's mass was measured using a polytech laser vibrometer, as shown in Figure 14. For each type, a mean value and the standard deviation were calculated. Table 5 shows the comparison between the simulated and measured resonance frequencies for the 3 different designs.

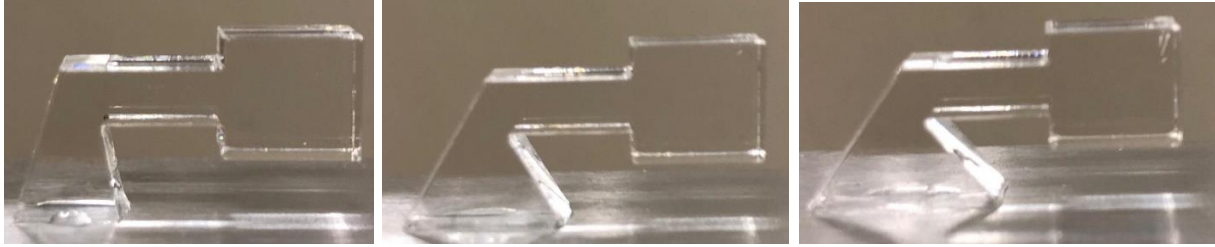


Figure 13: Samples of laser cut resonators (Left) Type 1 (Center) Type 2 (Right) Type 3.



Figure 14: Test set up to find the resonance frequency of the resonators.

Table 5: Comparison between the simulated and measured resonance frequencies for the 3 types of resonators.

Resonator	Numerical (Hz)	Experimental (Hz)	% Standard Deviation
Type 1	1673.97	1628 ± 9.50	0.58
Type 2	1669.97	1574 ± 17.9	1.13
Type 3	1672.93	1591 ± 25.8	1.62

By analyzing Table 5, it can be seen that the measured and averaged resonance frequencies are different than the ones numerically predicted. It has also been noticed that the % Standard Deviation, which is the ratio between the calculated standard deviation and the averaged resonance frequency, practically tripled when comparing resonator type 3 to resonator type 1. To check why it happened, one randomly chosen sample of each type of resonator was measured by a caliper to check the geometry. It has been verified that the dimensions of the realizable resonators do not match to those numerically designed, therefore, this explains why the resonance frequencies do not match either. Table 6 depicts the features of each type of resonator acquired by analyzing the

randomly chosen samples. Besides, not only the mismatch of resonance frequencies but also the fact that the % Standard Deviation increased from one resonator to another may have happened during the manufacturing process.

Table 6: Realized resonators' features.

Features	Resonator 1	Resonator 2	Resonator 3
Resonance Frequency [Hz]	1623.6	1586.8	1584.1
Static mass [g]	1.55	1.65	1.77
Effective mass [g]	0.808	0.833	0.832
SB limits [Hz]	1387 - 1644	1385 - 1627	1388 - 1626
SB Widths [Hz]	257	242	238
Length of Base [mm]	8.7	13.1	16
Footprint	21.75%	32.75%	40%

2.2.4. Experimentally testing the beams

Even though a mismatch was found between the resonance frequencies between the designed and realized resonators, beams were tested by adding the laser cut additions. As mentioned before, 4 beams were cut from the same aluminum panel in order to retain the same material properties. One beam was used as a bare case and the 3 others for the 3 types of resonators. As mentioned before, the free length of the beam considered in this report is 800 mm and the UC length is 40 mm, so that a total of 20 resonators were added to each beam. All of the resonators were placed with the center of their base in the center of the UC to avoid edge modes [12], as shown in Figure 15. The beams were clamped and vertically suspended, as shown in Figure 16.

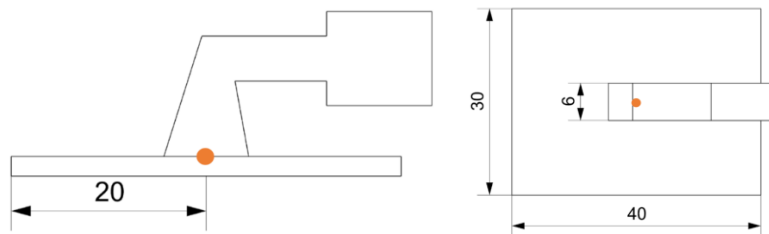


Figure 15: Example of a resonator type 1 placed on the center of the UC.

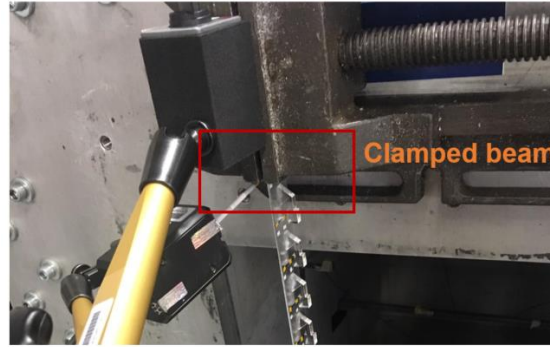


Figure 16: Beam clamped by a clamp at the sound box.

The beams were excited by utilizing an automatic impact hammer, kept always in the same position so the beams can have the same point of excitation, illustrated in Figure 17. The chosen point was placed as in the center of the beam as possible with the goal of exciting only flexural modes and avoiding that torsional modes get excited.

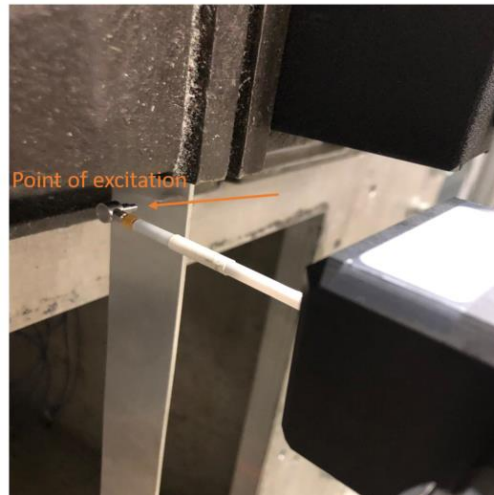


Figure 17: Automatic impact hammer set up to excite the beams.

Three points equally distributed in each of the 20 sections of the beams were used to acquire the vibration response due to the hammer excitation. The responses were acquired by using the PSV 500 laser vibrometer and calculating the RMS values of the Frequency Response Function (FRF) velocity/force per frequency through the response points, as shown in Figure 18.



Figure 18: (Left) Laser vibrometer (Right) Laser beam at a point to acquire the response in a beam.

Figure 19 depicts the comparison of FRFs between the bare beam and the beams with added resonators of the 3 types. The vertical lines represent the stop band limits predicted by using the randomly sampled resonators from Table 6 and they are colored according to the color of their respective curve e.g. the blue curve represents the FRF related to the beam with resonators type 1, thus, the blue vertical lines represent the predicted stop bands for the beam with resonators type 1, and so on.

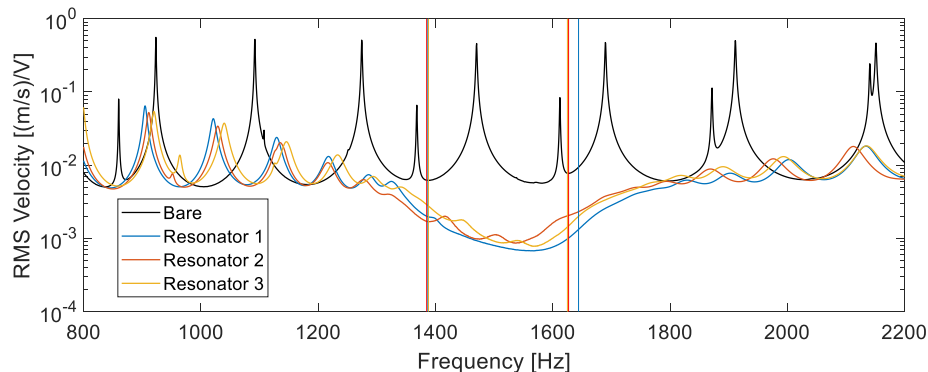


Figure 19: Comparison of experimental FRFs for the bare beam and the beams with resonators.

It can be seen that there was indeed an improvement in the vibration response where the stop bands were predicted for the 3 types of resonators. However, some expected trends could not be spotted. The trend of the curves shifting to higher frequencies could not be seen which is due to the fact that the laser cut resonators are not exactly tuned to the same resonance frequencies. In addition, some torsional modes were excited inside the predicted stop bands for the cases with resonators 2 and 3, which made it more difficult to assess whether or not the stop bands are becoming narrower

as the footprint increases. It can be that these torsional modes were excited because the point of excitation was not placed enough in the center. On the other hand, it can also be noticed that the response related to resonator type 1 outperform the other responses since it has a deeper dip.

2.3. Concluding remarks

In a nutshell, metamaterials have been investigated and proven to hold great potential to enhance the vibro-acoustic response of systems since they can create stop bands, which are frequency zones where free wave propagation is inhibited. Certain parameters seem to have some influence on these zones of pronounced attenuation. The footprint of a resonator has shown to be a parameter that not only affect their width but also their location in frequency domain.

On the one hand, the stop bands tend to be wider as the footprint of the resonant additions on the UC decreases. On the other hand, these zones tend to shift to higher frequencies as the value of the footprint increases. In this section, numerical as well as experimental results were shown in order to verify the influence of this parameter. From the results, it can be concluded that resonators with smaller footprints can outperform those with bigger footprints.

3. References

- [1] Claeys, C., et al. "Design and validation of metamaterials for multiple structural stop bands in waveguides." *Extreme Mechanics Letters* 12, 7-22 (2017).
- [2] Nateghi, Alireza, et al. "Wave propagation in locally resonant cylindrically curved metamaterial panels." *International Journal of Mechanical Sciences* 127, 73-90 (2017).
- [3] de Melo Filho, N. G. R., et al. "Dynamic mass based sound transmission loss prediction of vibro-acoustic metamaterial double panels applied to the mass-air-mass resonance." *Journal of Sound and Vibration* (2018).
- [4] Nouh, M., et al. "Wave propagation in metamaterial plates with periodic local resonances." *Journal of Sound and Vibration* 341 (2015): 53-73.
- [5] Van Belle, L., et al. "On the impact of damping on the dispersion curves of a locally resonant metamaterial: Modelling and experimental validation." *Journal of Sound and Vibration* 409, 1-23 (2017).
- [6] Krushynska, A. O., et al. "Towards optimal design of locally resonant acoustic metamaterials." *Journal of the Mechanics and Physics of Solids* 71, 179-196 (2014).
- [7] Sangiuliano, L; et al. W; 2017. "On the influence of boundary conditions on the predicted stop band width of finite size locally resonant metamaterials." 13th International Conference on Theoretical and Computational Acoustics, ICTCA 2017; 2017; Vol. 2017-July; pp. 99.
- [8] Liu, Z., et al. "Locally resonant sonic materials." *science* 289.5485 (2000).
- [9] Claeys, C., et al. "On the potential of tuned resonators to obtain low-frequency vibrational stop bands in periodic panels." *Journal of Sound and Vibration* 332.6 1418-1436 (2013).

- [10] Claeys, C. "Design and analysis of resonant metamaterials for acoustic insulation (Ontwerp en analyse van resonante metamaterialen voor geluidsisolatie)." (2014).
- [11] Liu, X. N., et al. "Wave propagation characterization and design of two-dimensional elastic chiral metacomposite." *Journal of Sound and Vibration* 330.11, 2536-2553 (2011).
- [12] Sangiuliano, L. et al. "Control of edge modes in finite vibro-acoustic resonant metamaterials." ISMA-USD Noise and Vibration Engineering Conference 2018.
- [13] Mace, B. R., et al. Modelling wave propagation in two-dimensional structures using finite element analysis, *Journal of Sound and Vibration*, Vol. 318, No. 4-5, 884-902 (2008).
- [14] Mead, D., Wave propagation in continuous periodic structures: research contributions from southampton, 1964-1995, *Journal of sound and vibration*, Vol. 190, No. 3, 495-524 (1996).
- [15] Mace, B. R., et al. Finite element prediction of wave motion in structural waveguides, *The Journal of the Acoustical Society of America*, Vol. 117, No. 5, 2835-2843 (2005).
- [16] Chen, J. S., et al. "Flexural wave propagation in metamaterial beams containing membrane-mass structures." *International Journal of Mechanical Sciences* 131, 500-506 (2017).